Structures 5 (2016) 196–206

Contents lists available at ScienceDirect

Structures

journal homepage: www.elsevier.com/locate/structures

Lateral Cyclic Behaviour of RC Columns Confined With Carbon Fibres

Pedro Faustino [a,*], Pedro Frade [a], Carlos Chastre [a,b]

[a] Department of Civil Engineering, Universidade NOVA de Lisboa, Portugal
[b] CEris, ICIST, Department of Civil Engineering, Universidade NOVA de Lisboa, Portugal

ARTICLE INFO

Article history:
Received 20 October 2015
Received in revised form 19 November 2015
Accepted 23 November 2015
Available online 2 December 2015

Keywords:
Carbon fibres
Confinement
Cyclic behaviour
Nonlinear modelling
Longitudinal strengthening
Reinforced concrete columns
Stainless steel

ABSTRACT

Reinforced concrete (RC) columns with various strengthening systems and different conditions were tested to cyclic lateral and axial loading for the purpose of performance assessment. Tests included confinement strengthening with carbon-fibre-reinforced polymer (CFRP) sheets, longitudinal strengthening with CFRP laminates and confining CFRP jacket, longitudinal strengthening with stainless steel bars and confining CFRP jacket, tested column until reinforcing steel failure, repair and CFRP confining jacket, and longitudinal strengthening with stainless steel bars. The analysis of the tests results as to load–displacement relationship and energy dissipation led to the conclusion that the use of external longitudinal strengthening with CFRP confinement is effective for performance retrofitting and upgrading, and viable in terms of execution. The load capacity increase due to strengthening reached 36–46% with good ductile behaviour. Nonlinear numerical modelling was carried out using two approaches which represent reasonably well the global performance of the studied columns for the prediction of the ascending load–displacement relationship and the peak load values in each cycle.

1. Introduction

Despite important experimental studies carried out in the past [1–7], which comprise essential data for the definition of predictive models, the numerical modelling of the nonlinear behaviour of structural elements remains a challenge. These studies were undertaken mostly to assess the performance of new RC columns under cyclic loading. Some include tests carried out on reinforced concrete (RC) columns with strengthening systems with the purpose of retrofitting or upgrading these elements in an undamaged state [2–6].

In order to widen the range of options and to understand whether these are feasible and effective, the present available data needs to be complemented with new test results as to the behaviour of RC columns strengthened with different combinations of systems and with different conditions, new or damaged.

In addition to the analysis of the experimental cyclic performance of RC columns, the numerical modelling of the behaviour of these elements is required so that design is fairly accurate in face of the real response of the columns. For this purpose, various authors have contributed to the development, assessment and calibration of numerical modelling approaches which do not seem to constitute yet a thorough contribution to the particular issue studied here [3,6–10].

This article presents the experimental results of 6 RC columns with different strengthening systems that include repair with high strength mortar, longitudinal external strengthening and external confinement under combined axial and lateral loads. The purpose is to assess the cyclic behaviour of these columns and, hence, contribute to the calibration of nonlinear modelling.

2. Experimental programme

2.1. Test specimens

The purpose of the experimental programme was to study the behaviour of rectangular RC columns strengthened with different techniques and materials in order to assess the improvement in their flexural response to combined lateral and axial loading. The RC columns were designed according to the Portuguese regulations – REBA 1967 [11] and REBAP 1983 [12] – still in effect in the 1980's, which did not include specific detailing requirements for seismic actions.

The dimensions and the reinforcement and strengthening detailing of the specimens are shown in Fig. 1. The summary of the strengthening systems is presented in Table 1.

In order to have a measurable reference, specimen P11ref was tested without strengthening and only to a certain extent beyond yielding (imposed displacement of 40 mm [2.3% drift ratio] in each direction). Specimen P12conf was confined with 3 layers of unidirectional CFRP sheets bonded to the concrete surface using the resin that would become the matrix of the composite.

Specimen P14rm_conf is the result of the strengthening of column P11ref after having been tested, which included the repair of the deteriorated length with an enhanced pre-mixed grout. The repair was carried out by cutting out an opening of approximately 55 mm depth,

* Corresponding author at: Mouchel — Scotland TranServ, Glasgow, Scotland, UK.

http://dx.doi.org/10.1016/j.istruc.2015.11.004
2352-0124/

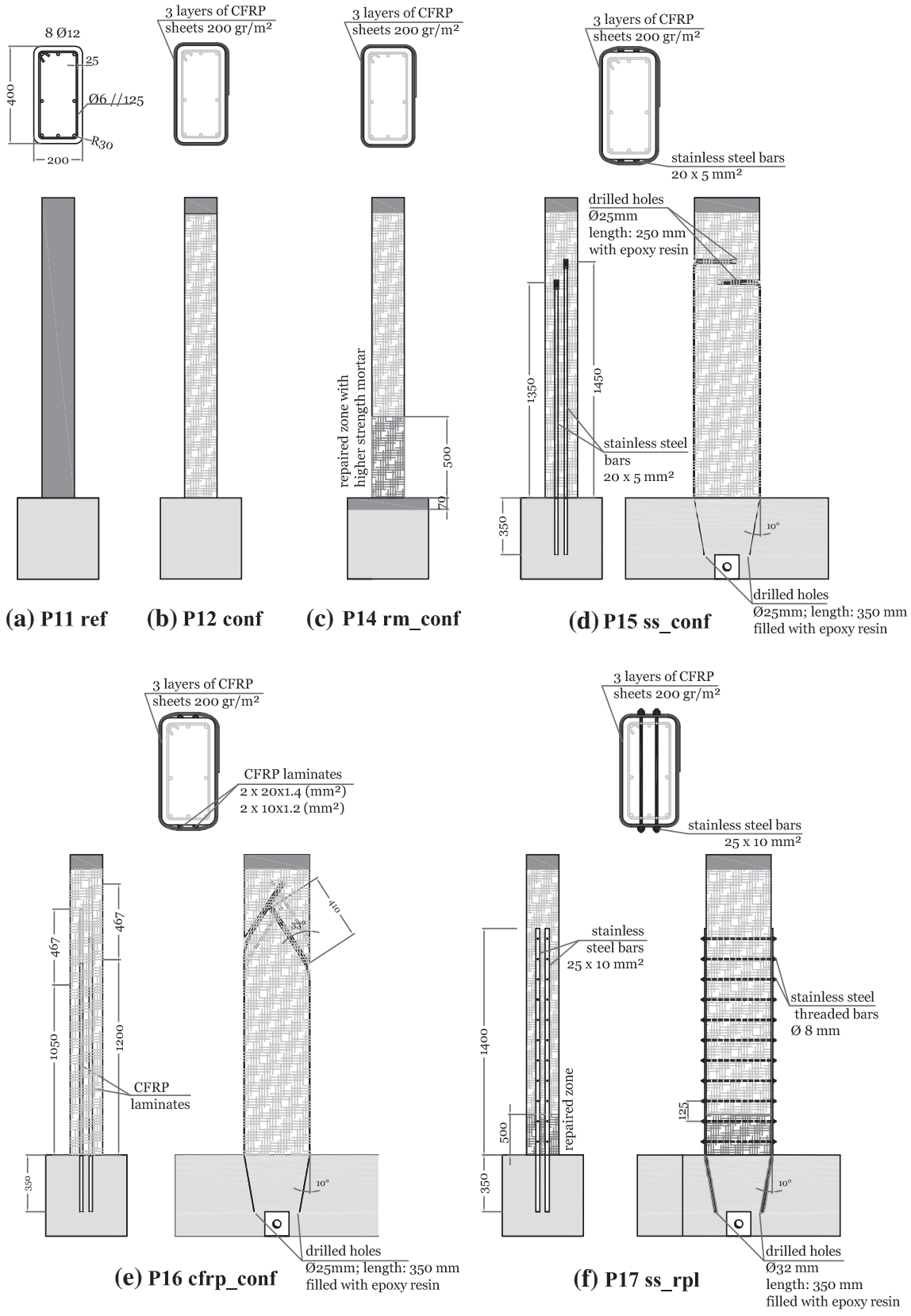

Fig. 1. Geometry, reinforcement and strengthening detailing of the tested columns: (a) P11ref; (b) P12conf; (c) P14rm_conf; (d) P15ss_conf; (e) P16cfro_conf; and (f) P17ss_rpl.

with a length of 500 mm from the bottom of the column, followed by the preparation of the surfaces, the application of the form work and the pouring of the grout.

Specimen P15ss_conf included two stainless steel longitudinal bars with 20 × 5 mm^2 on each smaller side dimension of the section, anchored at the bottom of the column in 10° inclined drilled holes in the

Table 1
Strengthening system for each column.[a, b, c]

Column	Condition before strengthening	Strengthening system	Axial Load, N (kN) [b]	N^b/N_R^c
P11 ref	New	None	320	0.18
P12 conf	New	- CFRP confinement: 3 layers	303	0.17
P14 rm_conf	Repaired/Strengthened after yielding of reinforcing steel	- Repair mortar along the length of the plastic hinge - CFRP confinement: 3 layers	308	0.13
P15 ss_conf	New	- 2 longitudinal bars on each side anchored in the footing block and in the top of columns in resin filled holes - CFRP confinement: 3 layers	305	0.14
P16 cfrp_conf	New	- 4 longitudinal CFRP laminates on each side anchored in the footing and in the top of columns in resin filled holes - CFRP confinement: 3 layers	306	0.13
P17 ss_rpl	Repaired/strengthened - Rupture of reinforcing steel on side A[a] - Yielding of reinforcing steel on side B[a]	- Repair mortar in half length of the plastic hinge - CFRP confinement: 3 layers - External stainless steel bars with equivalent strength to reinforcing steel	311	0.14

[a] side A — compression in push direction; side B — tension in push direction.
[b] N = axial load kept constant throughout the tests.
[c] N_R = axial strength of each column in kN.

footing block and at the top of the column in horizontal drilled holes. The holes were filled with an epoxy based adhesive. The column was then confined with three layers of CFRP jackets (200 g/m^2).

Specimen P16cfrp_conf was the result of a strengthening procedure similar to the previous column, although in this case the longitudinal strengthening was done with CFRP laminates. The anchoring of the laminates was carried out with epoxy adhesive and in holes with a 33° inclination from the vertical at the top of the column. The strengthening included on each smaller side of the column section 2 laminates of 20×1.4 mm^2 plus 2 laminates of 10×1.4 mm^2.

Specimen P17ss_rpl is the result of the strengthening of column P12conf and was tested until the longitudinal internal reinforcement broke along one of the sides. The deteriorated zone was repaired with an enhanced pre-mixed grout. The repair was carried out with grout in approximately 55 mm depth, along a length of 250 mm from the bottom of the column. The strengthening system was carried out using a similar procedure to that used on column P12conf, with 3 layers of bi-directional CFRP jacket (Figs. 1b and 2b). The strengthening system included two stainless steel bars with cross-section 25×10 mm^2 applied externally and anchored in drilled holes filled with a polymeric adhesive at the footing block and with 8 mm threaded bars crossing 12 mm diameter holes, anchored at their ends with nuts and torque of 25 Nm, passing through the largest dimension of the column along its length until the top with 125 mm spacing (Figs. 1f and 2f).

Table 2 presents the mean value results of the tested samples of the materials use in the specimens.

2.2. Test setup and instrumentation

The test setup is presented in Fig. 3 and consisted of a mechanical screw actuator of maximum horizontal load of 500 kN and maximum displacement of ±200 mm and a constant axial load of approximately 320 kN on the column throughout the test. All tests were displacement-controlled by an actuator and a load cell (TCLP TML-20B) with a capacity of 200 kN to measure the horizontal load. Each column was attached to the rigid floor by means of four post-tensioning bars. In all models the vertical load was kept constant during the test.

In all models the vertical load application system consisted of two post-tensioning bars fixed at the footing block of the column. The tensioning of both vertical bars through hydraulic cylinders created the desired constant axial load on the column. This axial load remained stable during the application of the horizontal displacements due to the use of the hydraulic pump which maintained the load constant throughout the entire test. The measurement of the vertical load was taken by two load cells with a capacity of 300 kN each.

The definition of the loading protocol was firstly approached based on the performance of the reference reinforced concrete column, P11ref. For this specimen the theoretical yield displacement Δ_y was calculated before the test took place, by means of Eq. (1) that is used in the Plastic Hinge Method [1], where φ_y is the yield curvature and L is the length of the column at which the load is applied.

$$\Delta_y \ \frac{1}{3} \ \varphi_y \ L^2 \tag{1}$$

The calculations were done considering the cross section response in bending with compression with an axial load of 300 kN and a yield strain ε_y of the reinforcing steel bars of 0.0023.

The calculated value of the yield curvature φ_y was of 0.0079 leading to a yield displacement Δ_y of 7.7 mm. In view of this, the definition of the imposed drift for column P11conf was established in 40 mm in both pull and push directions, so that the plastic branch behaviour of the column would be clearly installed and identified, as well as its peak load, P_{max}. After testing P11ref the yield displacements were identified as 8.8 mm in pull direction and 6.1 mm in push direction. The testing protocol for the remaining specimens included push–pull sets of cycles with a displacement increase of 15 mm until failure, twice the experimental mean yield displacement. Each displacement level comprised 3 cycles for each set of cycles.

The instrumentation setup is shown in Fig. 3b. The measurement of the horizontal displacement at the top of the column was done by a displacement transducer with a stroke of 500 mm and a sensitivity of 10×10^{-6}/mm. The horizontal and vertical displacements at the bottom of each column, which allowed determining the rotations, were measured using two sets of transducers: one with common LVDTs (TML CDP100 and CDP50) with strokes of 100 and 50 mm and sensitivities of 100×10^{-6}/mm and 200×10^{-6}/mm, respectively; the other set of transducers was with frames that include two rigid aluminium columns hinged to a flexible steel beam with four strain gauges that form a Wheatstone full bridge, having an amplitude of measurement of ±20 mm and a sensitivity of 250×10^{-6}/mm. The strain measurement in reinforcing steel (longitudinal and transverse), CFRP sheets, CFRP laminates and stainless steel was carried out through strain gauges with 5 mm length.

3. Tests results and discussion

3.1. Lateral load vs displacement — cyclic behaviour

Cyclic tests results in lateral load versus displacement are presented in Fig. 4 for all columns. The summary of results is expressed in Table 3. To compare the whole behaviour of the columns, the criteria of failure included either the break of steel reinforcement, which was observed in columns P12conf and P14rm_conf, or the decrease of the load, during the test, below 85% of maximum lateral load P_{max}, which was observed in column P17ss_rpl.

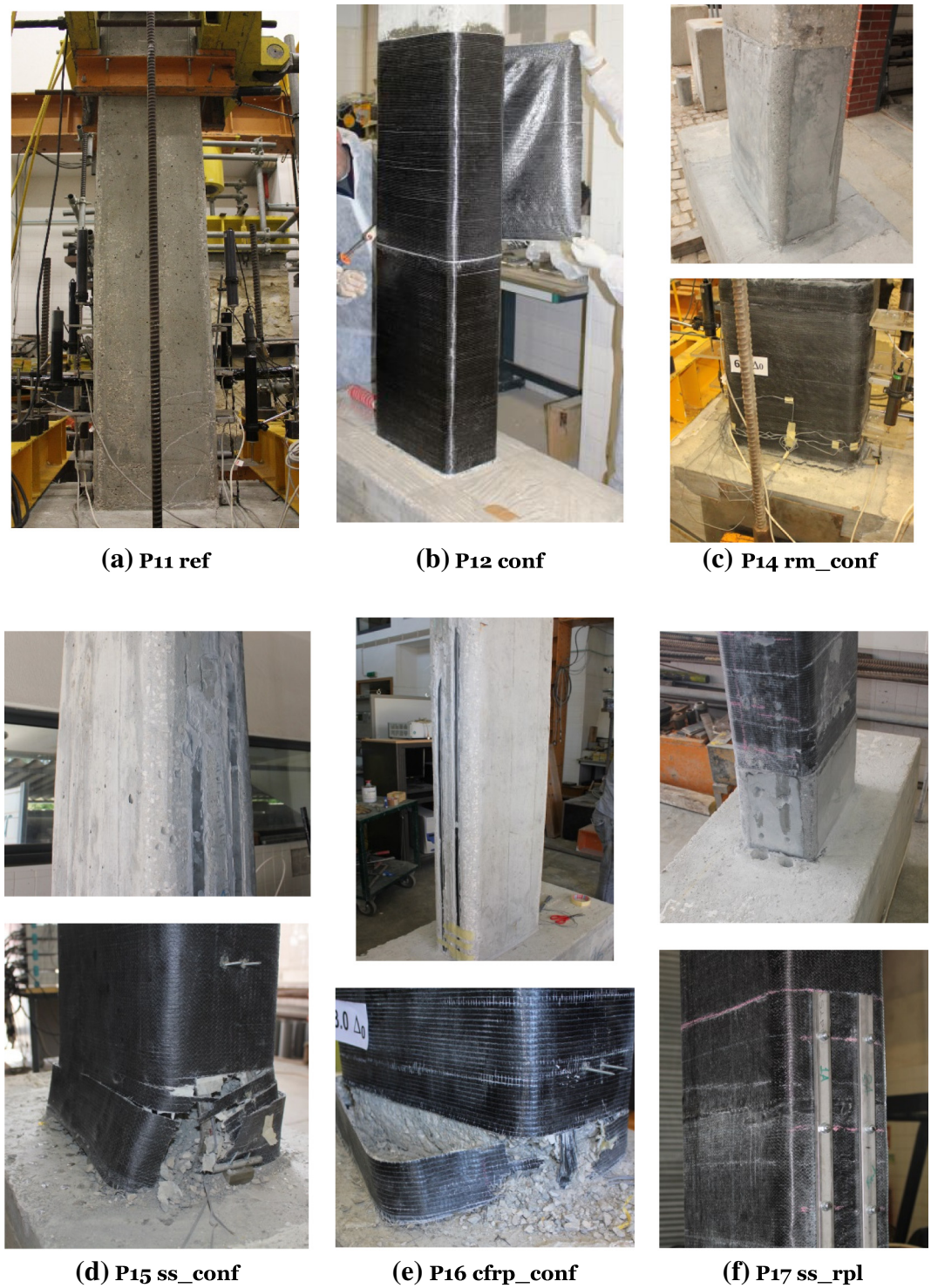

Fig. 2. Strengthening procedures for columns: (a) P12 conf; (b) P13 conf2; (c) P14 rm_conf; (d) P15ss_conf; (e) P16cfrp_conf; and (f) P17ss_rpl.

Table 2
Test results of the materials, mean values.

Column	P11ref	P12conf	P14rm_conf	P16cfrp_conf	P15ss_conf	P17ss_rpl
Concrete, f_c	25.8 MPa	26.5 MPa	30.8 MPa	34.1 MPa	33.5 MPa	32.9 MPa
Longitudinal steel	$f_y = 454$ MPa, $\varepsilon_u = 10.1\%$					
Transverse steel	$f_y = 580$ MPa, $\varepsilon_u = 6.0\%$					
CFRP sheets	–	$E_{CFRP} = 269$ GPa, $\varepsilon_u = 0.97\%$				
CFRP laminates	–	–		$E_{CFRP} = 159$ GPa $\varepsilon_u = 1.03\%$	–	–
Stainless steel	–	–		–	$f_y = 565$ MPa, $\varepsilon_u = 42.9\%$	
Repair mortar, f_c	–	–	59.0 MPa	–	–	59.0 MPa

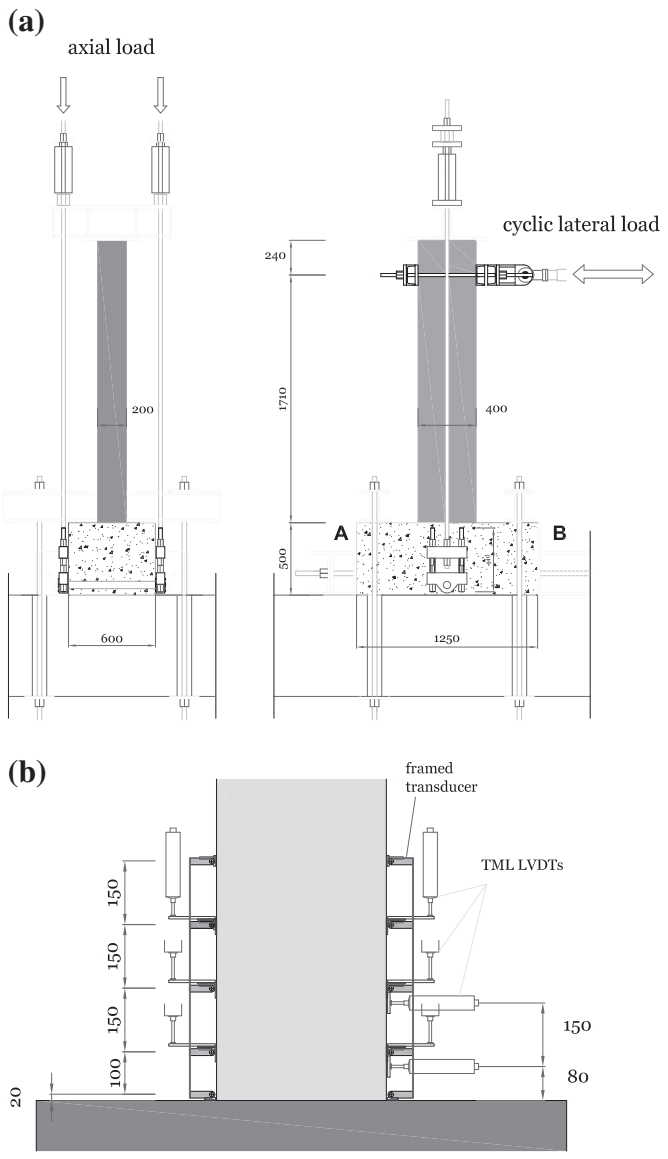

Fig. 3. (a) test setup; and (b) instrumentation.

Column P11ref presents a small difference between push and pull for the peak load, which in view of the remaining columns can be attributed to additional heterogeneities inherent to the specimen itself, other than the non-centred position of the longitudinal steel bars in the larger dimension of the column. Other possible reason for this difference was the cracking in the footing block, parallel to the lower side of the column, which was formed, before testing, during the pull of the post-tensioning vertical bars that fixed the whole specimen to the floor.

Fig. 4 shows that column P12conf has significant ductile behaviour compared with the remaining columns, with a drift ratio at break (ultimate drift ratio) of 7.0%, whereas the latter show a drift ratio of 4.4%. Moreover, in column P12conf the peak load value P_{max} is maintained throughout the test until failure, while the other strengthened columns present a strength degrading behaviour from the instant the peak load is attained. Nevertheless, the results of column P12conf show a peak load increase in view of the reference column P11ref of 7%, which is considerably lower than the strength increase obtained in the remaining columns which varies from 20% to 45%.

Even though column P14rm_conf presents a strength degrading behaviour, compared with column P12conf the peak load is higher, reaching an increase of 17%–20% compared with the reference specimen. The drift ratio at break reached 6.1%. The enhanced performance of specimen P14rm_conf can be explained by the presence of a higher strength compressive material – repair mortar – which may have reduced the cross section compressed area and therefore increased the internal lever arm between the compression and tension forces.

For column P15ss_conf the strengthening resulted in a peak load increase, compared with P11ref, between 35% and 41%, although the whole load–displacement relationship shows a strength degrading behaviour. During the test, column P15ss_conf did not show failure of any of the strengthening materials or reinforcing steel until a displacement of 45 mm – drift ratio of 2.6% – where the rupture of the CFRP confinement jacket took place at the base of the column. Until the end of the test neither the reinforcing steel nor the stainless steel bars reached failure. The test was stopped when the lateral load showed a value lower than 85% of the peak load, P_{max}.

In column P16cfrp_conf shows a strengthening ratio, considering the P11ref as reference, between 29% (pull) and 43% (push). The peak loads in the push and the pull direction were attained for drift ratios of 2.6% and 1.8% respectively. In the pull direction the rupture of both pairs of laminates took place in the 7th cycle, while in the push direction only one pair of laminates reached the rupture and at the 10th cycle. This explains the differences in both directions, as in the push direction the drop of loading is gradual from the 10th cycle until the failure criterion was reached, while in the pull direction the drop of the loading was sudden in the 7th cycle and from which the loading kept itself constant until failure. In the push direction the load–displacement behaviour may be described as strength degrading, while in the pull direction, after the sudden loss of strength the lateral load was nearly constant from the 7th cycle (1.8% drift ratio) to the 15th cycle (4.4% drift ratio).

The load–displacement relationship of column P17ss_rpl shows also a strength degrading behaviour. The peak load P_{max}, compared with the reference specimen P11ref, attained an increase value of 45% in the push direction and 20% in the pull direction. In the push direction the strength degrading behaviour was more evident. The reason for this is due to the presence of yielded reinforcing steel bars on the tensioned side of the column subject to push. On the opposite side, in the pull direction, the strength degradation was more gradual, where the longitudinal reinforcement bars were already broken.

3.2. Energy dissipation

Alongside the load–displacement analysis, the performance of the different strengthening systems is also evaluated as regards the energy dissipation.

Fig. 5a presents the dissipated energy in each single cycle – calculated as the area encircled by the load–displacement curve, while Fig. 5b presents the cumulative dissipated energy for each cycle – obtained from the sum of the areas of all previous cycles and in both graphs the peak loads are simultaneously displayed. From these figures it can be seen that there are no significant differences between all specimens, except for column P17ss_rpl, where the dissipated energy is slightly higher up to the 12th cycle. The remaining columns do not present relevant differences with regard to dissipated energy, either for each cycle or for cumulative values.

Fig. 5a shows the decrease of dissipated energy in each cycle within each set of cycles. The imposed displacement in the first cycle led the materials of the columns to a new strain level causing new cracks in the concrete, which means that for the following cycle the stiffness of the column was lower in the critical section. In this aspect there is no substantial difference between all columns.

Despite similar performance related to dissipated energy, all columns show different performance for lateral load capacity. Columns P12conf and P14rm_conf have lower load capacity and without significant variation all through the test. Opposite to these, columns P15ss_conf, P16cfrp_conf and P17ss_rpl have higher load capacity but globally decreasing during the test.

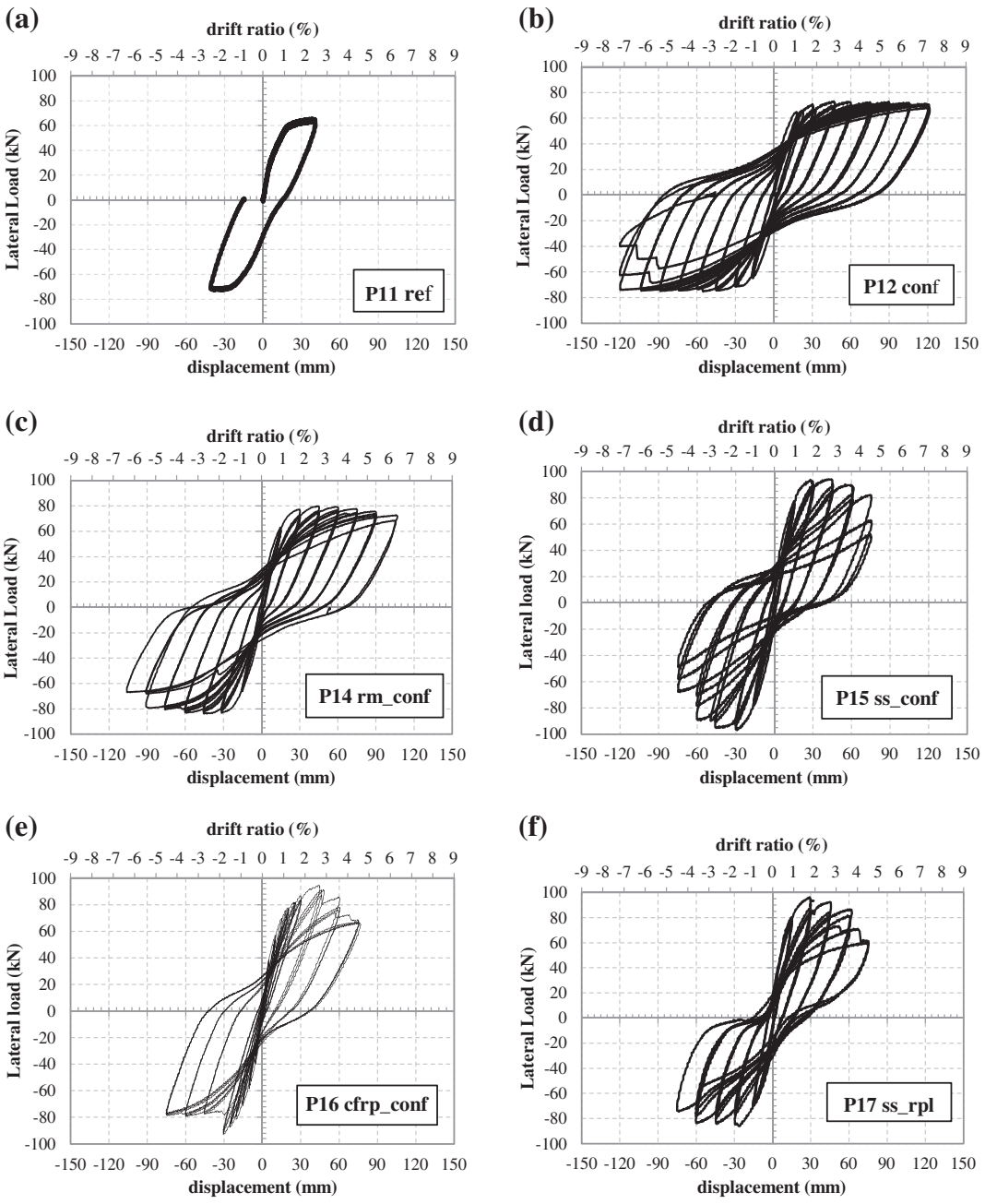

Fig. 4. Lateral load vs displacement: (a) P11ref; (b) P12conf; (c) P14rm_conf; (d) P15ss_conf; (e) P16cfrp_conf; and (f) P17ss_rpl.

4. Non-linear numerical modelling

This section presents two possible approaches to the modelling of the behaviour of the columns that were tested for axial and lateral loading using the finite element programme for nonlinear analysis of framed structures SeismoStruct v7.0 [13]. The programme includes different types of dynamic and static nonlinear analyses with an incremental iterative procedure and various types of frame elements. The displacement time-history applied to the top of the frame element was defined based on the testing data of column P12conf.

4.1. Distributed inelastic displacement-based frame element

The nonlinear analysis of frame elements through finite elements with displacement-based formulations has widely been used, although it has been indicated that the analysis based on such formulations tends to become outdated [14].

The displacement–based formulation is also known as stiffness formulation and its finite element approach consists of the interpolation of section deformations from an approximate displacement field followed by the use of the principle of virtual displacements (PVDs) to allow the equilibrium relationship. It needs to reduce its stiffness by increasing the number of element subdivisions.

This study used a subdivision of the frame element into six elements for a distributed inelastic displacement-based element where the frame elements were modelled with 250 section fibres.

4.2. Plastic-hinge inelastic force-based frame element

Concentrated inelasticity models are also called plastic-hinge models which consist of elastic elements in its length except in a

Table 3
Summary of results.

Column	Peak load, P_{max}, kN		Peak moment, M_{max}, kNm		Strengthening ratio		Yield displacement, Δy[a] mm (%)[c]		Displ. at break[b],Δu mm (%)[a]
	Push	Pull	Push	Pull	Push	Pull	Push	Pull	
P11 ref	66.5	72.0	111.4	123.8	1.00	1.00	8.8 (0.51%)	6.1 (0.36%)	–[d]
P12 conf	73.0	75.2	124.9	128.6	1.10	1.04	8.5 (0.50%)	7.9 (0.46%)	120 (7.0%)
P14 rm_conf	79.9	84.0	136.6	143.7	1.20	1.17	9.8 (0.57%)	10.2 (0.60%)	105 (6.1%)
P15 ss_conf	94.1	97.0	160.0	164.8	1.41	1.35	9.1 (0.53%)	7.6 (0.44%)	75 (4.4%)
P16 cfrp_conf	94.8	92.9	162.1	158.8	1.43	1.29	8.0 (0.47%)	8.6 (0.50%)	75 (4.4%)
P17 ss_rpl	96.1	87.0	163.3	146.2	1.45	1.20	8.6 (0.50%)	9.9 (0.58%)	75 (4.4%)

[a] Drift ratio: displacement at the point of load application divided by the column length from the base to this point.
[b] Δy was calculated using the bilinear approximation presented by Hose and Seible [1].
[c] In column P17ss_rpl the ultimate displacement was the one corresponding to less than 85% P_{max}.
[d] Similar tested columns [6,7] showed drift ratios at failure of approximately 3%.

determined fixed length where the distributed inelasticity is concentrated. In this case the formulation of this inelasticity is force-based.

The initial plastic hinge length used in the mathematical models was estimated based on the expression proposed by Priestley and Park [15] where $lp = 0.08\,L + 0.022\,f_s\,d_s$ with lp being the plastic hinge length, f_s the steel yield stress and d_s the diameter of the longitudinal steel reinforcement. Other authors propose different models specific for the estimation of the length of plastic hinge in FRP confined columns [16,17,18]. However, given that the mathematical models wold then be adjusted to the behaviour of the tested columns, the authors opted to use the Priestley and Park equation for an initial estimate. The value of 257 mm was obtained, which is 15% of the length L of the column.

After calibration of the models taking account of the tests results, the plastic hinge length of the columns P15ss_conf, P16cfrp_conf and P17ss_rpl, strengthened with longitudinal CFRP laminates or with stainless steel bars and confined with CFRP jackets, was reviewed and defined as 12% of the total length. This value corresponds to the empirical assumption that the length of the plastic hinge, in a reinforced concrete column, corresponds approximately to half of the side of the cross-section. In this case this value is 200 mm, which corresponds to 11.7%.

Table 4 shows the plastic-hinge length adopted for each model that represents the tested columns in view of the best fit to the experimental results.

4.3. Properties of the materials

The study examines the structural behaviour of reinforced concrete columns that were strengthened with different materials. It takes into account the complexity of the nonlinear behaviour of the materials, excluding CFRP whose stress–strain relationship is linear up to rupture, the numerical modelling of the tested columns makes it necessary to resort to material constitutive models that can contribute to a reliable estimation of their behaviour.

The different constitutive models are described in this section and the corresponding parameters were defined or adapted according to the modelling results that best fit the results of the material tests.

4.3.1. Concrete

The model that was adopted for the nonlinear behaviour of the reinforced concrete is based on the stress–strain relationship defined by Mander et al. [19] and the cyclic procedure proposed by Martinez-Rueda and Elnashai [20].

The input parameters are presented in Table 5. For what is here defined as 'unconfined' concrete and based on what was proposed by Mander et al. [19] the model includes the confinement effect that the transverse reinforcing steel grants to the cross-section.

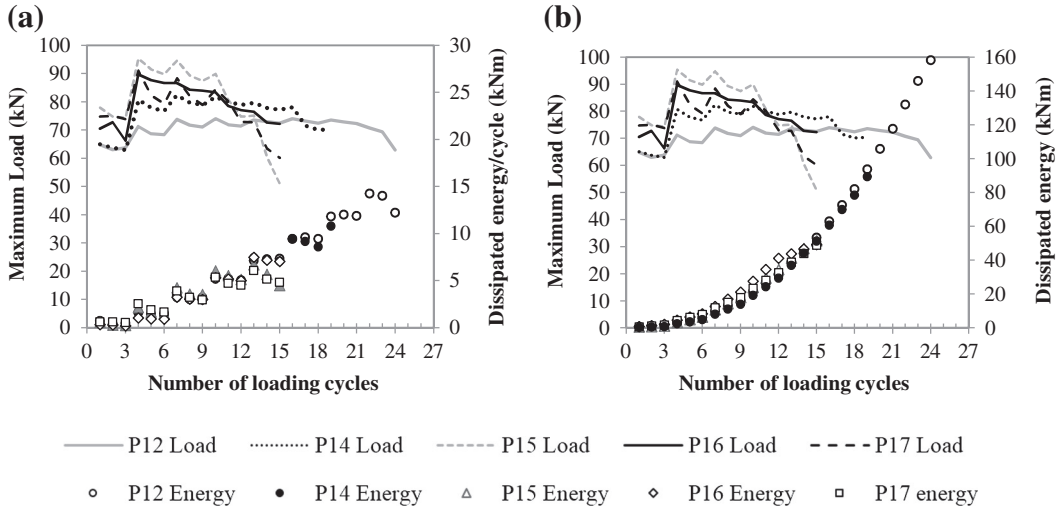

Fig. 5. Dissipated energy and lateral load versus number of cycles: (a) per cycle; and (b) cumulative.

Table 4
Plastic-hinge length modelled for each column as a percentage of total length (1.71 m).

	P11 ref	P12 conf	P14 rm_conf	P15 ss_conf	P16 cfrp_conf	P17 ss_rpl
Plastic-hinge length	15%	15%	15%	12%	12%	12%

With regard to the confinement provided by the external jacketing of the CFRP sheets, which is referred to as 'confined' concrete, the envelope curve of Mander et al. model is modified by Faustino et al. model [21] whose model was created for CFRP confined square sections under axial compression. Despite the studied columns are rectangular and under the effect of bending with compression, the authors opted to maintain the numerical analysis considering Faustino et al. model.

4.3.2. Reinforcing steel

The nonlinear uniaxial model adopted for the reinforcing steel is based on the stress–strain relationship of Menegotto and Pinto [19] together with the isotropic hardening equations defined by Filippou et al. [23]. The advantage of this model in relation to the bilinear elasto-plastic model is that it includes the Bauschinger effect, which better represents the behaviour of reinforcing steel under cyclic loading where stiffness degradation needs to be represented.

The parameters necessary for the definition of this model are the steel yield strength, the modulus of elasticity, the strain-hardening ratio μ and the parameters regarding the transition of the curve from elastic to plastic behaviour, which are represented in Table 6. The mechanical parameters were obtained from tested samples prior to the execution of the columns.

4.3.3. Stainless steel for longitudinal strengthening

For stainless steel the nonlinear model that was adopted was the same as for reinforcing steel, based on Menegotto and Pinto [22] coupled with Filippou et al. [23]. However, apart from the yield strength, some of the parameters were changed in order to take into account the specific behaviour of this material with regard to the transition between the elastic and plastic behaviour. The input variables for the numerical model are presented in Table 7.

The change in the values of the transition parameters in relation to the reinforcing steel was due to the fact that stainless steel has a significantly gradual transition between the elastic branch and the post yielding branch. The quantification of these values was carried out taking into account the results of the tests carried out on columns P15ss_conf and P17ss_rpl.

Table 6
Mechanical parameters of the reinforcing steel for the numerical model.

Yield strength	Elasticity modulus	Strain hardening	Transition curve parameters				
f_y (MPa)	E_s (GPa)	μ	*R0*	*A1*	*A2*	*A3*	*A4*
452	200	0.0044	20.5	19.0	0.15	0.025	1.0

4.3.4. CFRP laminates for longitudinal strengthening

Composite materials such as fibre reinforced plastics show a linear elastic behaviour up to rupture when subjected to uniaxial loading in tension. The adopted model is a simplified uniaxial trilinear law without strength in compression.

The parameters needed for the definition of the numerical model are the mechanical properties of the FRP material represented by the elasticity modulus E_f and the ultimate tensile strength f_f. The values of these parameters were obtained from the testing of samples resulting in a mean value of the elasticity modulus of 159 GPa and a mean value of the ultimate axial strain of 1.03% which corresponds to a mean tensile strength of 1637 MPa.

5. Modelling results vs experimental results

The numerical modelling of the cyclic behaviour of the columns presented in this study was undertaken based on their actual geometric and detailing properties along with the properties of all the materials with the corresponding models described in the previous section.

Using two approaches, the modelling results were compared with the tests results for columns P11ref, P12conf, P14rm_conf, P15ss_conf, P16cfrp_conf and P17ss_rpl in terms of cyclic performance of load–displacement relationship and the envelope of load–displacement relationship for different drift ratios.

5.1. Load vs displacement cyclic behaviour

The overall results that compare tests with numerical modelling are shown in Fig. 6. The reference column P11ref is a particular case (Fig. 6a) where a displacement of approximately 40 mm was imposed on one cycle in each direction. For the remaining columns the analysis shows the cyclic behaviour up to the criteria of failure adopted to define the test ultimate displacement.

For P11ref it can be seen that the modelling results of both approaches do not seem to match the test curve. In addition to the difference in the unloading path, the second branch of the modelling curves presents softening behaviour during loading, while the test curve shows hardening behaviour. When positioning the column in place for testing, the irregular lower face of the footing block should have been

Table 5
Mechanical parameters of the concrete for the numerical model.

Column	Strengthening type	Unconfined concrete			Confined concrete		
		Comp. strength f_{c0} (MPa)	Tensile strength f_{to} (MPa)	Strain at comp. peak stress ε_{co} (m/m)	Peak comp. stress f_{cc} (MPa)	Peak tensile stress f_{tc} (MPa)	Strain at comp. peak stress ε_{cc} (m/m)
P11ref	Reference column	20.6	1.6	0.0035	–	–	–
P12conf	3 CFRP sheets	21.5	1.7	0.0022	23.5	1.8	0.006
P14rm_conf [a]	3 CFRP sheets + repaired with mortar	24.6	1.7	0.0022	59.1	4.1	0.0035
P15ss_conf	3 CFRP sheets + long. stainless steel	26.8	1.9	0.0022	29.1	2.1	0.007
P16cfrp_conf	3 CFRP sheets + long CFRP laminates	27.3	1.9	0.0022	29.6	2.2	0.007
P17ss_rpl	3 CFRP sheets + repaired with mortar + longstainless steel	26.3	1.8	0.0022	28.6	2.1	0.007

[a] P14rm_conf was repaired with a high strength mortar. The adopted concrete parameters for the section were those of concrete confined with CFRP sheets assuming the compressive and tension strength of the mortar.

Table 7
Mechanical parameters of the stainless steel for the numerical model.

Yield strength	Elasticity modulus	Strain hardening	Transition curve parameters				
f_y (MPa)	E_s (GPa)	μ	*R0*	*A1*	*A2*	*A3*	*A4*
565	200	0.00135	19.5	19.0	0.15	0	1.0

placed against an additional relatively resilient material over the floor slab, such as gypsum, which was used in the other tests. As a result, while tensioning the vertical bars to fix the footing block to the floor slab, the footing block cracked at a distant of approximately 25 cm from the column on both sides. These cracks changed the actual length of the column as the restraining length went deeper in the footing block. Taking into consideration the curves of both modelling approaches, it can be seen that these show some differences, especially in the push direction.

In column P12conf the lateral load is slightly underestimated by the modelling approaches when compared to test results in both directions from 6% to 10%. The modelling curves show significantly higher stiffness in the unloading path, which might be explained by the non-consideration of the buckling of reinforcing steel in the compressed

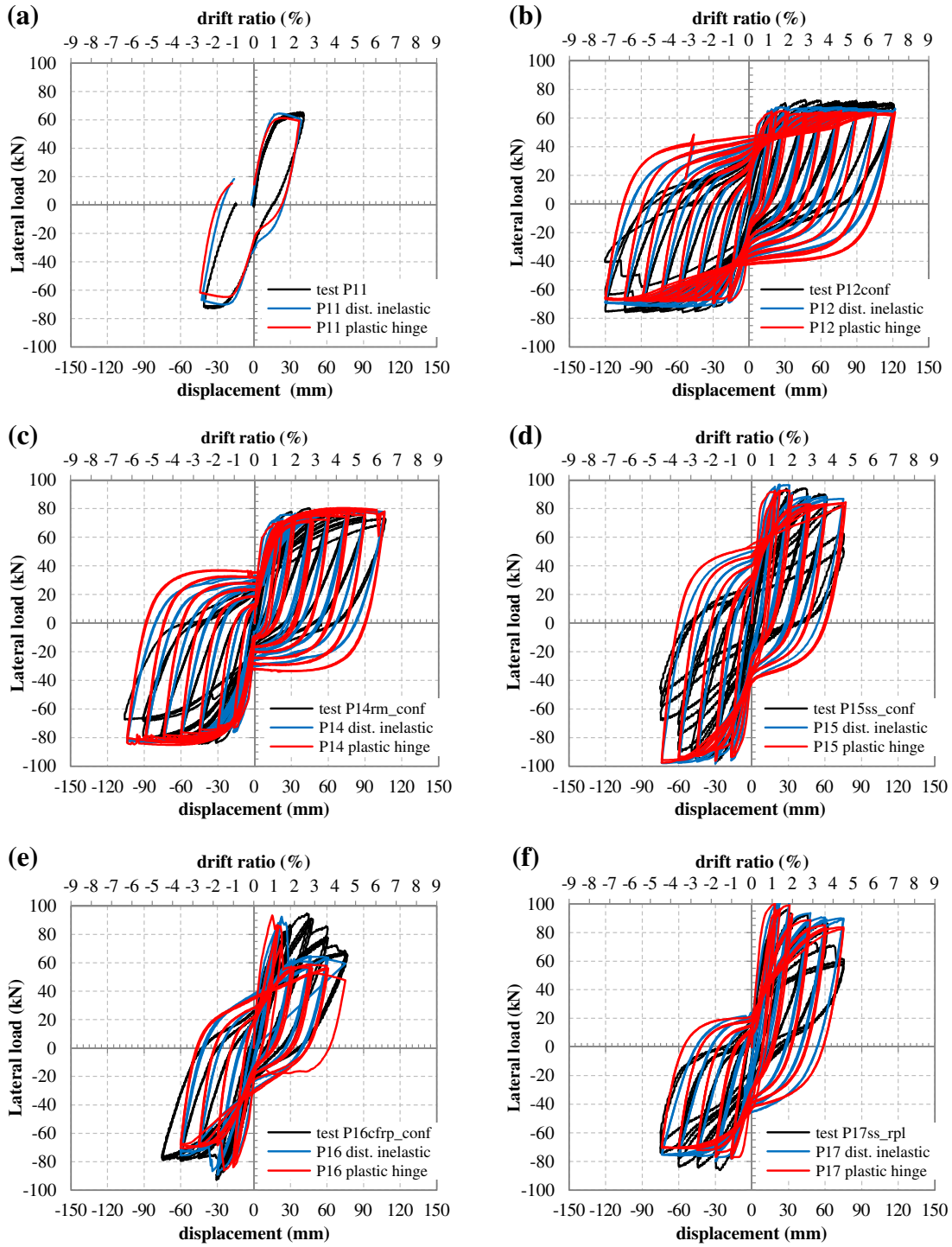

Fig. 6. Cyclic behaviour lateral load vs imposed displacement for columns: a) P11ref; b) P12conf; c) P14rm_conf; and d) P15ss_conf; P16cfrp_conf; P17ss_repl.

side of the column. When comparing both modelling approaches, the model with distributed inelasticity in displacement-based elements shows results closer to those expressed in the experimental curve while the plastic-hinge force-based approach presents an unloading path with even higher stiffness.

For P14rm_conf the modelling curves show similar behaviour to the test curve considering the peak load in each cycle from 30 mm displacement onward. The peak load between all curves varies up to approximately 5%. Nevertheless, the slopes of the first branch of both loading and unloading paths are significantly higher for both modelling curves in relation to the test curve.

In column P15ss_conf the difference of peak loads between numerical modelling results and test results vary from 1% to 3%. It can be said that there is a fair approximation to the test curve although, for this column also, the same difference is observed to have a significantly higher stiffness behaviour expressed in the unloading branch of both modelling curves. The final cycle shows a significant reduction in the load capacity for the test curve, although the numerical models were unable to replicate it. This aspect is likely to be associated with the stainless steel material modelling. The definition of the parameters that model the transition from linear-elastic to inelastic behaviour is difficult with some of the available models [22,24,25]. As regards the comparison of both modelling approaches, the plastic-hinge approach shows slightly less peak load values for each cycle and a higher unloading slope, representing higher stiffness at this stage.

In column P16cfrp_conf the modelling curves seem to be relatively close to the test curve in the pull direction as shown in Fig. 6. In the push direction the test shows an increase in its load capacity until the CFRP laminate rupture at an imposed displacement of 45 mm (2.6% drift ratio). In the pull direction the rupture of the laminates was reached at an imposed displacement of 30 mm (1.8% drift ratio). Consequently, the behaviour of the column in the push direction presents a gradual decrease of the lateral load for each cycle after the rupture of the laminates. From the modelling results it is interesting to observe that in both approaches the estimated behaviour in both directions is similar. In normal circumstances a symmetrical behaviour would be expected for the column subjected to cyclic testing. It is assumed that this non-symmetrical behaviour, taking into account pull and push directions, is due to either geometrical or material heterogeneities or even both. In any case the peak lateral load of test and modelling curves vary in the range of 1% to 3%.

Column P17ss_rpl had rupture of the longitudinal reinforcing steel on one side and yielding on the opposite side. The particularity of the analysis of this column is due to less load capacity in the push direction. Both modelling approaches realistically represent the behaviour of the column where the peak load in each cycle varied between 1% and 5%. However, in the pull direction this difference reached 10%. This modelling difficulty is likely to be related to the models that define both types of steel, i.e., the reinforcing mild steel and the stainless steel. To model more effectively the behaviour in the presence of both types of steel, the calibration of the global numerical modelling reduced its accuracy to the case where there is no contribution from the reinforcing steel but only from the strengthening stainless steel.

6. Conclusions

The longitudinal strengthening of columns resulted in the increase of the load capacity – approximately 40% – although the ductility capacity decreased compared with the columns without this strengthening. Furthermore, these all columns showed a strength degrading behaviour until failure, while the column only with the confinement strengthening maintained its load capacity until rupture. Even so, failure took place for imposed displacements corresponding to drift ratios of more than 4%, considered as high displacement values for what most structures should bear.

As to the performance of the materials, in all the columns the concrete crushed at an early stage of the cyclic loading and the rupture of the longitudinal reinforcing steel was observed in the subsequent cycles, except in one of the columns. The CFRP laminates, applied to one of the columns and anchored at both ends, also reached rupture at an early stage of the cyclic loading. As for the stainless steel in two of the tested columns, the strengthening bars did not reach rupture, given the highly ductile behaviour of this material.

Based on the experimental results, two modelling approaches were implemented to predict the behaviour of concrete columns under axial and lateral loading with different condition and strengthening solutions with different materials.

The calibration of both modelling approaches was carried out in order to simulate the complete cyclic behaviour of the columns taking into consideration not only the peak load but also the complete performance until failure. Taking into account the peak lateral load in each column, the values of both modelling results compared with the tests results vary from 1% to 10%. The numerical model using distributed inelastic frame elements shows slightly better accuracy for most columns in all behaviour relationships and parameters. The plastic-hinge approach presents globally lower values of the peak load in each cycle.

References

[1] Hose YD, Seible F. "Performance evaluation database for concrete bridge components and systems under simulated seismic loads". PEER Report 1999/11. San Diego: Pacific Earthquake Engineering Research Center; 1999.
[2] Bousias SN, Triantafillou TC, Fardis MN, Spathis L, O'Regan BA. "Fiber reinforced polymer retrofitting of rectangular reinforced concrete columns with or without corrosion". ACI Struct J 2004;101(4) (512_20).
[3] Chastre C. Comportamento às acções cíclicas de pilares de betão armado reforçados com materiais compósitos. PhD thesis. Universidade NOVA de Lisboa Lisbon; 2005[in Portuguese].
[4] Barros J, Varma R, Matta F, Sena-Cruz J, Lignola GP, Azevedo A. Near surface mounted CFRP strips for the flexural strengthening of RC columns. Experimental and numerical research. Eng Struct 2008;30:112–23.
[5] Bournas DA, Triantafillou TC, Zygouris K, Stavropoulos F. Textile-reinforced mortar versus FRP jacketing in seismic retrofitting of RC columns with continuous or lap-spliced deformed bars. J Compos Constr 2009;13:360–71.
[6] Rocha P. Retrofitting and rebuilding of reinforced concrete columns of buildings in seismic zones". PhD thesis (in Portuguese). Portugal: University of Porto; 2011.
[7] Rodrigues H. Biaxial seismic behaviour of reinforced concrete columns". PhD thesis. Portugal: University of Aveiro; 2012.
[8] D'Ambrisi A, Filippou FC. Modeling of cyclic shear behavior in RC members. J Struct Eng Am Soc Civ Eng Oct. 1999;125(10):1143–50.
[9] Bousias SN, Panagiotakos TB, Fardis MN. Modelling of RC members under cyclic biaxial flexure and axial force. J Earthq Eng 2002;6:213–38.
[10] Desprez C, Mazars J, Kotronis P, Paultre P. Damage model for FRP-confined concrete columns cyclic loading. Eng Struct 2013;48:519–31.
[11] REBA. "Regulamento de estruturas de betão armado ((Regulation for Reinforced Concrete Structures)"). Decree nr 599/67 ; July 25 1976[in Portuguese].
[12] REBAP. "Regulamento de estruturas de betão armado e Pré-esforçado ((Regulation for Reinforced and Prestressed Concrete Structures)"). Decree-Law nr 349-C/83 ; July 30 1983[in Portuguese].
[13] Seismosoft. "SeismoStruct v7.0 — a computer program for static and dynamic nonlinear analysis of framed structures"; 2014available from http://www.seismosoft.com.
[14] Correia A, Almeida J, Pinho R. Force-based versus displacement-based formulations in the cyclic nonlinear analysis of RC frames. The 14th World Conference On Earthquake Engineering. Beijing, China: NICEE; October 12-17 2008.
[15] Priestley MJN, Park R. Strength and ductility of concrete bridges columns under seismic loading. ACI Struct J 1987;84(8):61–76.
[16] Mortezaei A, Ronagh HR. Plastic hinge length of FRP strengthening reinforced concrete columns subjected to both far-fault and near-fault ground motions. Sci Iran A 2012;16(6):1365–78.
[17] Jiang C, Wu Y, Wu G. Plastic hinge length of FRP-confined square RC columns. J Compos Constr 2014;18(4).
[18] Youssf O, ElGawardy MA, Mills JE. Displacement and plastic hinge length of FRP-confined circular reinforced concrete columns. Eng Struct 2015;101:465–76.
[19] Mander JB, Priestley MJN, Park R. Theoretical stress–strain model for confined concrete. J Struct Eng 1988;114(8):1804–26.
[20] Martinez-Rueda JE, Elnashai AS. Confined concrete model under cyclic load. Mater Struct 1997;30(197):139–47.
[21] Faustino P, Chastre C, Paula R. Design model for square RC columns under compression confined with CFRP. Composites Part B 2014;57:187–98.
[22] Menegotto M, Pinto PE. Method of analysis for cyclically loaded R.C. plane frames including changes in geometry and non-elastic behaviour of elements under combined normal force and bending. Symposium on the Resistance and Ultimate

Deformability of Structures Acted on by Well Defined Repeated Loads. Zurich Switzerland: International Association for Bridge and Structural Engineering; 1973. p. 15–22.
[23] Filippou FC, Popov EP, Bertero VV. Effects of bond deterioration on hysteretic behaviour of reinforced concrete joints. Report EERC 83-19. Earthquake Engineering Research Center. Berkeley: University of California; 1983.
[24] Dodd L, Restrepo-Posada J. Model for predicting cyclic behavior of reinforcing steel. J Struct Eng 1995;121(3):433–45.
[25] Monti G, Nuti C. Nonlinear cyclic behaviour of reinforcing bars including buckling. J Struct Eng 1992;118(12):3268–84.